Ecological Modelling 321 (2016) 10–22

Contents lists available at ScienceDirect

Ecological Modelling

journal homepage: www.elsevier.com/locate/ecolmodel

A HMM-based model to geolocate pelagic fish from high-resolution individual temperature and depth histories: European sea bass as a case study

Mathieu Woillez[a,*], Ronan Fablet[b], Tran-Thanh Ngo[a,c], Maxime Lalire[a,d], Pascal Lazure[e], Hélène de Pontual[a]

[a] Ifremer, Sciences et Technologies Halieutiques, CS 10070, 29280 Plouzané, France
[b] Institut Telecom/Telecom Bretagne, UMR 6285 LabSTICC, CS 83818, 29238 Brest CEDEX 3, France
[c] Université de Strasbourg, ICube UMR 7357, BP 10413, 67412 Illkirch Cedex, France
[d] CLS, Space Oceanography Division, 8-10 rue Hermes, 31520 Ramonville Saint-Agne, France
[e] Ifremer, Laboratoire de Physique Hydrodynamique et Sédimentaire, CS 10070, 29280 Plouzané, France

ARTICLE INFO

Article history:
Received 4 May 2015
Received in revised form 9 October 2015
Accepted 10 October 2015
Available online 4 December 2015

Keywords:
Fish movement
Archival tagging
Migration
Population structure
Hidden Markov Model (HMM)
State-space model

ABSTRACT

Numerous methods have been developed to geolocate fish from data storage tags. Whereas demersal species have been tracked using tide-driven geolocation models, pelagic species which undertake extensive migrations have been mainly tracked using light-based models. Here, we present a new HMM-based model that infers pelagic fish positions from the sole use of high-resolution temperature and depth histories. A key contribution of our framework lies in model parameter inference (diffusion coefficient and noise parameters with respect to the reference geophysical fields—satellite SST and temperatures derived from the MARS3D hydrodynamic model), which improves model robustness. As a case study, we consider long time series of data storage tags (DSTs) deployed on European sea bass for which individual migration tracks are reconstructed for the first time. We performed a sensitivity analysis on synthetic and real data in order to assess the robustness of the reconstructed tracks with respect to model parameters, chosen reference geophysical fields and the knowledge of fish recapture position. Model assumptions and future directions are discussed. Finally, our model opens new avenues for the reconstruction and analysis of migratory patterns of many other pelagic species in relatively contrasted geophysical environments.

1. Introduction

Tagging experiments have been widely developed for the geolocation and tracking of animals in movement ecology studies. Classically, global positioning systems (GPS) are used to track seabirds or mammals including marine mammals. However, geolocation remains complex for fish. Either acoustic telemetry studies are undertaken to track small-scale displacements in space, or geolocation studies are performed using error-prone locations derived from light, depth and temperature collected from pop-up satellite archival tags (PSATs) (e.g., tuna in Royer et al., 2005) or tide signal collected from data storage tags (DSTs) (e.g., cod in Pedersen et al., 2008). These techniques are well adapted for fish either exhibiting trans-oceanic migration, or having low activity where tide can be retrieved from a pressure sensor. For other species, the challenge of geolocating and tracking fish from individual environmental histories remains and relies on our ability of correlating individual fish histories to environmental spatio-temporal fields derived for instance from satellite observations and/or operational hydrodynamic models. This is the case of the European sea bass (*Dicentrarchus labrax*). Despite its high economical and societal value, little is known about the spatial dynamics of this species at the population scale, and yet this information is necessary to better manage this likely overexploited stock (ICES, 2015).

From a methodological point of view, the reconstruction of tracks of animals generally relies on a state-space modeling framework. It states the geolocation and tracking as the inference of the hidden sequence of positions (referred to as 'states') from the available sequence of observations. As the movement of the fish is a continuous process in space and time, continuous settings along with Kalman (Sibert et al., 2003) or particle filters (Royer et al., 2005; Breed et al., 2012) are natural. However, discrete settings associated with Hidden Markov Models may provide relevant alternatives regarding calibration and inference issues

* Corresponding author. Tel.: +33 0 2 29 00 85 65; fax: +33 0 2 29 00 85 47.
E-mail address: mathieu.woillez@ifremer.fr (M. Woillez).

http://dx.doi.org/10.1016/j.ecolmodel.2015.10.024

(Pedersen et al., 2008). Overall, state-space model involves two key components: a dynamical model and an observation model. The dynamical model (i.e., the model for the movement of the fish) generally exploits generic random walk models, e.g., Brownian motion (Holgate, 1971) or correlated random walks (Bovet and Benhamou, 1988). The observation model depends on the targeted applications and should relate the recorded data to the hidden states. Whereas the observation model is straightforward with GPS tags, no such explicit relationships can be analytically found when considering undersea geolocation. Previous works have explored specific observation models for fish geolocation using depth histories for demersal species for regions involving strong tide signals (Pedersen et al., 2008) as well as light measurements for pelagic species for tropical latitudes (Royer et al., 2005). To our knowledge, the geolocation of fish, such as sea bass involving both demersal and pelagic behaviors, remains a challenge.

In this paper, we address the geolocation of pelagic fish from individual depth and temperature histories. Our methodological contribution is two-fold: (i) defining a relevant observation model at a daily scale to match individual temperature/depth fish histories to modeled and/or observed environmental conditions, (ii) extending the discrete HMM-based setting proposed by Pedersen et al. (2008) to address a joint calibration and inference of the considered model. In this model, only the primary parameters, i.e., the ones required to effectively geolocate the fish (the movement rate or diffusion and the temperature related parameters), are estimated, while the other ones like the parameters related to the depth and release/recapture position were considered determined or with a fixed uncertainty. As a case-study, we consider the European sea bass and report experiments on both numerical simulations and real DST data. These experiments demonstrate the robustness of the considered model and numerical implementation as well as the feasibility of the DST-based geolocation of pelagic fish. We further discuss the key features of our model as well as the expected contributions to behavioral fish ecology.

2. Material and methods

2.1. DST data

Adult sea bass were internally tagged with DSTs (CEFAS G5 long live). Tagging operations were carried out in summer for 3 consecutive years (2010–2012) in the Iroise Sea, off the west coast of Brittany (France). Logging regimes were tested over the different years; all presented a high acquisition rate (temperature and depth at 1′ interval during the first year post-tagging, reduced to 5′–10′ for the second year). Daily range of vertical movements can be high (Fig. MM1) and in most cases, the fish experienced temperatures equivalent to either sea surface temperature (SST; at depth <10 m) and/or sea bottom temperature (SBT; at depth >40–50 m) during the same day.

2.2. Geophysical fields

The geolocation model considers three geophysical fields: SST derived either from a satellite-based observation or from a hydrodynamic model, the SBT and the bottom depth both derived from the same hydrodynamic model. The model outputs were obtained from the French MARS model of IFREMER (Lazure et al., 2009; Lazure and Dumas, 2008). It provided series of maps with a $4\,\mathrm{km} \times 4\,\mathrm{km}$ resolution. The satellite-based SST observations were extracted from the Odyssea NWE product (Piolle et al., 2010). This product is a gridded and interpolated field (i.e., missing-data-free) derived from a multi-sensor analysis with a $0.02^\circ \times 0.02^\circ$ resolution. For consistency, the satellite-based observations were re-interpolated over the MARS grid. The MARS domain was reduced in longitude to 11°W to 2°E, and in latitude to 43°N to 52°N, but it was kept large enough to encompass any trajectory reconstruction. From comparison to in situ data, the typical levels of uncertainty (in standard deviation unit) were 0.65 °C for SST derived from the satellite-based observation (Piolle et al., 2010), and 1.0 °C for temperatures derived from the hydrodynamic model (Lazure et al., 2009). For the SST, differences exist between the two types of geophysical fields as illustrated by the field anomaly computed for a given day (Fig. MM2). As the typical level of uncertainty of satellite-based observations is lower than that of the hydrodynamic model, the trajectory patterns reconstructed using the satellite-based observations may be more constrained by the very values recorded by the tag than those using inputs from the hydrodynamic model. However, the uncertainty between these two reference geophysical fields is neither homogeneous in space, as seen on the anomaly map for a given day (Fig. MM2), nor in time. Thus, a sensitivity analysis has been performed on the geophysical reference fields by reconstructing trajectories using either satellite-derived SST or MARS SST (see Section 3.3).

2.3. HMM-based geolocation model

The geolocation problem is stated as an inference based on the Bayes theorem within a state-space framework. Let us denote by $X=(X_t)$ the position series in the 2-dimensional geographical space to be inferred at a daily resolution and $Y=(T_t,D_t)$ the observed histories of temperature (T_t) and depth ($\underline{D}_t$) retrieved from DSTs. Hereafter, X will be referred to as the hidden state sequence. It might be stressed that, for geolocation problems, the state may also include speed and direction variables in addition to position variables (Jonsen et al., 2005; Breed et al., 2012).

Here, subscript t refers to daily time indices from the release ($t=0$) of the tagged fish to its recapture ($t=N-1$). It may be noted that depth and temperature histories are acquired at a high-resolution such that variable T_t (resp. D_t) refers to all temperature (resp. depth) measurements stored by the DST during day t. We use the standard convention that day t starts at midnight.

The state-space model involves two key components: the dynamical model and the observation model (Fig. MM3). The dynamical model describes the time dynamics of the state sequence. We resort to a Brownian random walk model described by:

$$X_{t+1} = X_t + N_t \tag{1}$$

where, N_t is a white Gaussian noise with (isotropic) diagonal covariance $\Sigma = \sigma_D^2 I$. The standard deviation σ_D relates to the Brownian diffusion as $\sigma_D^2 = 2D\Delta t$ with D the diffusion coefficient (in $\mathrm{km}^2/\mathrm{day}$) and Δt the time (here daily) step (Risken, 1996; Pedersen et al., 2008). Hence, the diffusion coefficient D characterizes the mean distance covered by the fish daily. More precisely, for a Brownian random walk, the mean speed relates to the standard deviation σ_D as follows $\bar{v} = \sqrt{0.5\pi\sigma_D^2}$. Thus, the mean distance covered by the fish (in km/day) equals $\sqrt{\pi D}$. The Brownian random walk model amounts to stating the hidden sequence as a first-order Markov chain, where the dynamical model (1) defines the conditional transition $P(X_{t+1}|X_t)$ from current state X_t to next state X_{t+1}.

The observation model resorts to defining observation likelihood $P(Y_t|X_t)$. At each time t, it evaluates the extent to which observation Y_t and state X_t are coherent. Whereas, in most geolocation models, one can exploit an analytically-derived relationship between the observation and the state (e.g., the Kalman filter for the bigeye tuna (Sibert et al., 2003), the particle filter for the bluefin tuna (Royer et al., 2005)), no such relationship can be derived in our

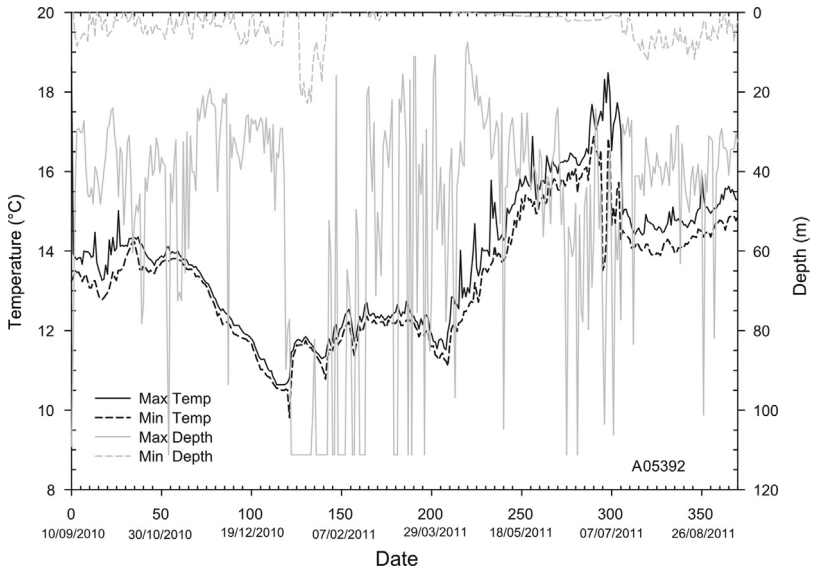

Fig. MM1. DST data: daily summary (min and max data) of temperature and depth series for a representative fish (tag A05392). During winter, a plateau at c.a. 114 m (data below this depth limit were truncated due to DST tag specification) indicates that deeper depths were experienced by this fish although the literature indicates a maximum of 100 m (Frimodt, 1995).

case between the depth and temperature series at time t and the spatial position of the fish. Our idea is to evaluate whether or not depth and temperature measurements Y_t conform to the expected temperature and bathymetry conditions at position X_t. Formally, let us denote by $\mathrm{SST}_{\mathrm{SAT}}(X_t)$ the satellite-derived SST at position X_t, $T_{\mathrm{MARS}}(X_t)$ the MARS-derived temperature profile from the sea surface to the sea bottom at position X_t and $D_{\mathrm{BATHY}}(X_t)$ the depth of the sea bottom at position X_t. Observation likelihood $P(Y_t|X_t)$ is stated as the product of a bathymetry-driven term and a temperature-driven term:

$$P(Y_t|X_t) = P(D_t|D_{\mathrm{BATHY}}(X_t)) \times P(T_t|D_t, \mathrm{SST}_{\mathrm{SAT}}(X_t), T_{\mathrm{MARS}}(X_t)) \quad (2)$$

The bathymetry-driven term amounts to discarding positions for which the depth of the sea bottom is below the depth experienced by the fish.

$$P(D_t|D_{\mathrm{BATHY}}(X_t)) = \begin{cases} 1 \text{ if } D_{\mathrm{BATHY}}(X_t) \geq D_t^{\max} \\ 0 \text{ otherwise} \end{cases} \quad (3)$$

where, $D_t^{\max}$ is the maximum depth experienced by the fish during day t.

Regarding the temperature-driven term, we exploit the behavioral pattern of sea bass. Three different daily behavioral patterns have been described in the wild by Quayle et al. (2009) but in most cases fish typically explore the water column from the surface to the sea bed within a same day. Such behavior was also experimentally observed by Schurmann et al. (1998). Given the vertical stratification in the considered study area (Lazure et al., 2009), one can then expect the fish to depict significant time periods below and above the thermocline. Hence, at a given position X_t, the temperature-driven term evaluates whether or not the temperatures experienced by the fish close to the sea surface and below the thermocline conform to the satellite-derived and MARS-derived temperature conditions respectively.

where, G_σ stands for a zero-mean Gaussian distribution with standard deviation σ, $\sigma_{\mathrm{surface}}$ the standard deviation of the sea surface term and σ_{bottom} the standard deviation of the sea bottom term. $\mathrm{SST}(T_t, D_t)$ and $\mathrm{SBT}(T_t, D_t)$ are respectively proxies of the sea surface temperature and sea bottom temperature in the area explored by the fish at day t. Given the vertical distribution of the thermocline in the study area (Koutsikopoulos and Le Cann, 1996), we consider as surface layer depths between 0 m and 10 m and bottom layer depths below 50 m for months September to December, and below 40 m for the rest of the year. We then define $\mathrm{SST}(T_t, D_t)$ as the maximum temperature experienced by the fish at day t for depth values lower than 10 m and $\mathrm{SBT}(T_t, D_t)$ as the minimum temperature experienced by the fish at day t for depth greater than 50 m for months September to December, and greater than 40 m for the rest of the year. It may be noted that, in some areas in winter, the sea surface layer may involve colder temperatures than the bottom (Koutsikopoulos and Le Cann, 1996). To account for such temperature patterns, $\mathrm{SST}(T_t, D_t)$ becomes a minimum of the temperature values in the surface layer and $\mathrm{SBT}(T_t, D_t)$ a maximum of the temperature values in the bottom layer. However, if the fish is neither in the surface layer nor in the bottom layer at day t, the temperature-driven term is equally probable over the entire domain. It is noteworthy that, at the surface, satellite-derived temperature conditions in Eq. (4) could be replaced without changes by MARS-derived temperature conditions in order to perform a sensitivity analysis on the geophysical reference fields (see Section 3.3).

Regarding the release and the recapture position, the geolocation model treats them differently. For the recapture position, either this position is known and the observation likelihood for the last day is multiply by a bivariate Gaussian error centered on the recapture position with a variance chosen *a priori* to $(0.1/\mathrm{h})^2$ (h being the grid resolution, i.e., 4 km), or this position is not known and the observation likelihood for the last day remains unchanged.

$$P(T_t|D_t, \mathrm{SST}_{\mathrm{SAT}}(X_t), T_{\mathrm{MARS}}(X_t)) = \begin{cases} G_{\sigma_{\mathrm{surface}}}(\max(\mathrm{SST}(T_t, D_t)) - \mathrm{SST}_{\mathrm{SAT}}(X_t)) \times G_{\sigma_{bottom}}(\min(\mathrm{SBT}(T_t, D_t)) - \mathrm{SBT}_{\mathrm{MARS}}(X_t)) \\ \text{if } SST_{SAT}(X_t) \geq SBT_{MARS}(X_t), \\ G_{\sigma_{\mathrm{surface}}}(\min(\mathrm{SST}(T_t, D_t)) - \mathrm{SST}_{\mathrm{SAT}}(X_t)) \times G_{\sigma_{bottom}}(\max(\mathrm{SBT}(T_t, D_t)) - \mathrm{SBT}_{\mathrm{MARS}}(X_t)) \\ \text{else } \mathrm{SST}_{\mathrm{SAT}}(X_t) < \mathrm{SBT}_{\mathrm{MARS}}(X_t). \end{cases} \quad (4)$$

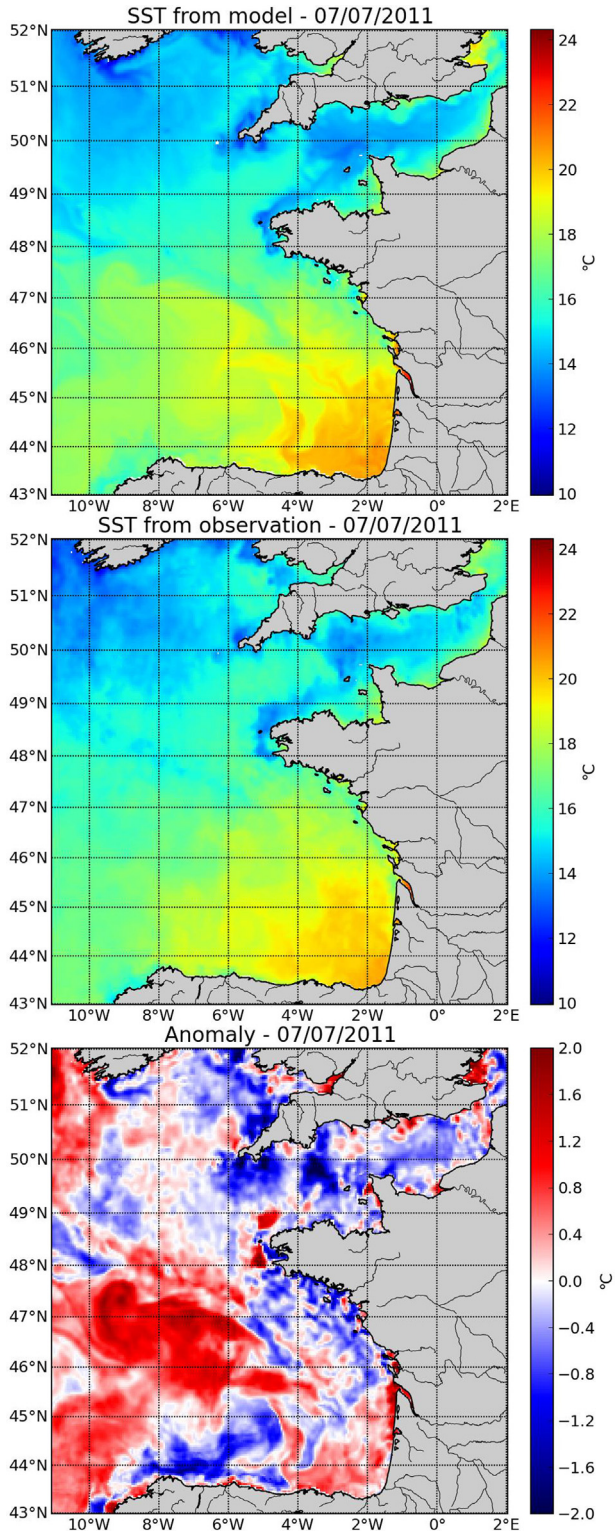

Fig. MM2. (Top) SST from the satellite. (Middle) SST from the model MARS 3D. (Bottom) SST anomaly between satellite and model MARS 3D (For interpretation of the references to color in this figure legend, the reader is referred to the web version of this article).

The release position is known by definition and there is no uncertainty associated to it.

2.4. Model calibration and inference

Given the proposed state-space model, the geolocation problem resorts to an inference based on the Bayes theorem. For a given fish, it amounts to evaluate the posterior probability of the state sequence (i.e., track) given the DST data from the release of the fish to its recapture. The additional knowledge of the release and/or recapture positions might also be considered in the inference. Different numerical schemes may be considered to evaluate the posterior. Among them, Kalman methods and particle filtering are the most popular methods (Sibert et al., 2003; Nielsen et al., 2006; Johnson et al., 2008). Kalman methods only apply to linear Gaussian observation and dynamical models and cannot be considered in our case, as the observation model does not involve a linear relationship between the state and the observations (Eq. (4)). Particle filters (e.g., Royer et al., 2005; Breed et al., 2012) are appealing to account for non-linear and non-Gaussian models at the expense however of an increased computational cost, especially for the evaluation of the so-called smoothing posterior distribution $P\left(X_t|(Y_{t'})_{t'=0:N-1}\right)$ of the state X_t conditionally to all observations (and not only observations up to time t).

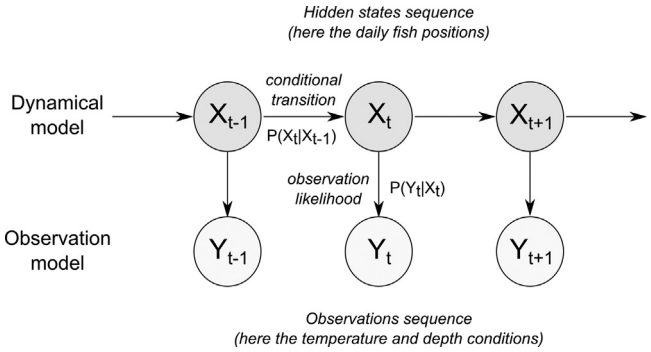

Fig. MM3. Conceptual diagram of the HMM-based geolocation model.

Recently Pedersen et al. (2008) explored a discretized solution of the geolocation based on discrete Hidden Markov Model (HMM). Rather than considering continuous positions, it comes to constraining the positions on a discrete grid. The state then evolves in a discrete space, whose cardinal is the number of possible locations on the discrete grid. Within this discrete setting, one can exploit classical forward-backward HMM (Baum et al., 1970; Rabiner, 1989), which provides an exact computation of the filtering and smoothing posterior distributions, $P\left(X_t|(Y_{t'})_{t'=0:t}\right)$ and $P\left(X_t|(Y_{t'})_{t'=0:N-1}\right)$. We let the reader refer to Pedersen (2007) for the details of the forward–backward procedure. As by-products, given model parameters, one can derive both:

- the MAP (Maximum A Posteriori) as the sequence X_t obtained using the Viterbi algorithm (Viterbi, 1967; Forney, 1973)

$$\hat{X}^{\mathrm{MAP}} = \underset{X}{\operatorname{argmax}}\ P\left((X_t)_{t=0:N-1}|(Y_t)_{t=0:N-1}, \Theta\right) \tag{5}$$

  where, Θ refers to model parameter D, $\sigma_{\mathrm{surface}}$ and σ_{bottom}.
- the MPM (Maximum Posterior Mode) as the sequence $\hat{X}_t^{\mathrm{MPM}}$ verifying at time t

$$\hat{X}_t^{\mathrm{MPM}} = \underset{X_t}{\operatorname{argmax}}\ P\left(X_t|(Y_{t'})_{t'=0:N-1}, \Theta\right) \tag{6}$$

  The MPM sequence minimizes the estimation variance, i.e., the variance of the estimation error (Robert, 2007).
- the Mean Posterior as the sequence $\hat{X}_t^{\mathrm{MP}}$ verifying at time t

$$\hat{X}_t^{\mathrm{MP}} = E\left[X_t|(Y_{t'})_{t'=0:N-1}, \Theta\right] \tag{7}$$

- representative sequence examples $\left(X^{(i)}\right)$ from the sampling of the posterior likelihood

$$X^{(i)} \sim P\left((X_t)_{t=0:N-1}|(Y_t)_{t=0:N-1}, \Theta\right) \tag{8}$$

It may be noted that, in the continuous case, for non-Gaussian/non-linear settings, one cannot derive analytically nor computationally any of these expressions. Particle filtering may only provide a mean to approximate these estimates and distributions (Doucet et al., 2000; Royer et al., 2005).

Here, we follow the discrete setting proposed by Pedersen et al. (2008) for our geolocation model. Besides, we further investigate model calibration issues. Overall, our model involves three parameters, namely the diffusion coefficient D of the dynamical model and the standard deviations of surface and bottom temperature model, σ_{surface} and σ_{bottom}. In Pedersen et al. (2008), the authors only consider the Maximum Likelihood (ML) calibration of the dynamical model using a gradient-based maximization. By contrast, we further exploit the computational properties of the discrete setting and address a joint ML estimation of all model parameters using an iterative Expectation-Maximization (EM) framework (Dempster et al., 1977). It provides a simple and robust implementation of the ML inference (Do and Batzoglou, 2008). Formally, at iteration k, it comes to iteratively solve for the maximization of the expectation of the joint log-likelihood of the observation and state sequences conditionally to the posterior distribution of the state sequence for the current parameter estimates.

$$\hat{\Theta} = \underset{\Theta}{\text{argmax}} E_{X|Y,\Theta^{(k)}}\left[\log p\left((Y_t)_{t=0:N-1}, (X_t)_{t=0:N-1}|\Theta\right)\right] \tag{9}$$

Maximization (9) can be regarded as a reweighted ML criterion where the posterior distribution acts as a weighing factor. The great interest of the EM algorithm is that it delivers a two-step iterative algorithm: the E-step computes the posterior distribution $P\left((X_t)_{t=0:N-1}|(Y_t)_{t=0:N-1}\right)$ given current model parameter estimates; and the M-step updates model parameters according to a ML criterion reweighted by the posterior distribution. The EM algorithm (Do and Batzoglou, 2008) guarantees to increase the likelihood after each EM iteration and as such it can be regarded as a gradient-based procedure. However, their convergence depends on the initial parameter values. To improve the robustness to the initialization, we consider here a stochastic version of the EM algorithm, the Stochastic EM (SEM) procedure (Diebolt et al., 1994). It replaces the numerical evaluation of the posterior distribution $P\left((X_t)_{t=0:N-1}|(Y_t)_{t=0:N-1}, \Theta^{(\nu)}\right)$ in the E-step by its sampling. Here, this sampling exploits the classical HMM forward–backward procedure (see Pedersen, 2007). Overall, at iteration k, the SEM procedure involves two steps:

- **the E-step** comes to sampling N_{SEM} trajectories $\left(X^{(i)}\right)_{i=1:N_{\text{SEM}}}$ from posterior $P\left(X|Y, \Theta^{(\nu)}\right)$ using the standard forward–backward HMM procedure (Rabiner, 1989; Pedersen, 2007);
- **the M-step** comes to updating estimate $\Theta^{(\nu+1)} = \left(D^{(\nu+1)}, \sigma^{(\nu+1)}_{\text{surface}}, \sigma^{(\nu+1)}_{\text{bottom}}\right)$ as

$$\begin{aligned} D^{(\nu+1)} &= \frac{1}{4N_{\text{SEM}}N}\sum_{i=1}^{N_{\text{SEM}}}\sum_{t=0}^{N-1}\left(X^{(i)}_{t+1} - X^{(i)}_{t}\right)^2 \\ \sigma^{(\nu+1)}_{\text{surface}} &= \sqrt{\frac{1}{N_{\text{SEM}}N}\sum_{i=1}^{N_{\text{SEM}}}\sum_{t=0}^{N-1}\left(\text{SST}(X_t, T_t, D_t) - \text{SST}_{\text{SAT}}\left(X^{(i)}_t\right)\right)^2} \\ \sigma^{(\nu+1)}_{\text{bottom}} &= \sqrt{\frac{1}{N_{\text{SEM}}N}\sum_{i=1}^{N_{\text{SEM}}}\sum_{t=0}^{N-1}\left(\text{SBT}(X_t, T_t, D_t) - \text{SST}_{\text{MARS}}\left(X^{(i)}_t\right)\right)^2} \end{aligned} \tag{10}$$

Updates (10) refer to classical ML parameter estimation applied to the sampled trajectories $\left(X^{(i)}_t\right)$. We let the reader refer to Appendix 1 for the details of the derivation of these updates. This two-step SEM procedure is iterated until convergence (ratio between the average over the 20 last values of D and the new value of D below 1%). The SEM procedure can be regarded as a stochastic gradient-based scheme with improved convergence to the global estimate compared to classical EM or gradient-based algorithms (Diebolt et al., 1994). In addition, the proposed SEM procedure estimates both the diffusion coefficient and the observation errors, while the gradient-based ML setting considered in Pedersen et al. (2008) only estimates the diffusion coefficient, the observation errors being set *a priori*. Regarding its computational complexity, it relates to the number of sampled trajectory according to posterior distribution $P\left((X_t)_{t=0:N-1}|(Y_t)_{t=0:N-1}, \Theta^{(\nu)}\right)$. By contrast, the computational complexity of gradient-based methods depends more heavily on the size of the discrete grid of possible locations.

2.5. Evaluation of the model performance

With the aim of evaluating the robustness of our geolocation model, synthetic data were generated with a diffusion coefficient of 30.0 km^2/day and observation errors (in standard deviation) of 1.0 °C for sea bottom temperature and 0.65 °C for sea surface temperature (in agreement with the typical level of uncertainty of the reference geophysical fields). The synthetic data involve the simulation of sequences of positions (longitude, latitude) and depths over a 150-day time series. The simulated trajectory is generated using a random walk with the chosen diffusion coefficient, a release point in the Iroise Sea (48.5°N, 4.0°W), and a linear drift (1.5° toward South and 0.9° toward East). The simulated depths were drawn independently for each given day from a multinomial distribution with a probability mass function of 0.2 for the fish being at the surface only, 0.2 for the fish being at bottom only and 0.6 for the fish being at the surface and at the bottom. On these synthetic data, the gradient-based inference introduced in Pedersen et al. (2008) and the proposed SEM-based inference were compared.

For the real data, a similar comparison was performed. In addition, a sensitivity analysis was undertaken. The objective was to evaluate and understand how the various model parameters, the geophysical reference fields and the recapture location influence the reconstruction of the trajectories.

3. Results

3.1. Model calibration and inference for synthetic data

One hundred synthetic track data were simulated following our simulation procedure. All the simulated trajectories spread over the continental shelf of the Bay of Biscay and showed a southward migration in the Bay of Biscay (cf. an example simulated trajectory in Fig. R1). Model calibration and inference were performed using both the SEM procedure and the gradient-based ML approach proposed by Pedersen et al. (2008). The SEM procedure was run until convergence. The estimated parameters were considered as the average values over the last 20 iterations. The SEM procedure converged for all the synthetic track data. For an example of the synthetic data (Fig. R1), the estimated diffusion coefficient (33.8 km^2/day) and the estimated observation errors (1.070 °C for the sea bottom temperature and 0.697 °C for the sea surface temperature) were close to the simulated true values (Table R1). In addition, the reconstructed trajectory patterns (the posterior distribution summed over time, the mean, the modal and the most probable tracks) were in agreement with the simulated trajectory (Fig. R2). With observation errors set to the simulated true values or to the SEM estimates, the gradient-based ML estimates of D were respectively 32.4 km^2/day and 31.2 km^2/day, corresponding to relative differences with the SEM estimate of 7.7% and 4.1% smaller, respectively. Both estimates were close to the SEM estimate (Table R1), showing that both techniques were coherent. The

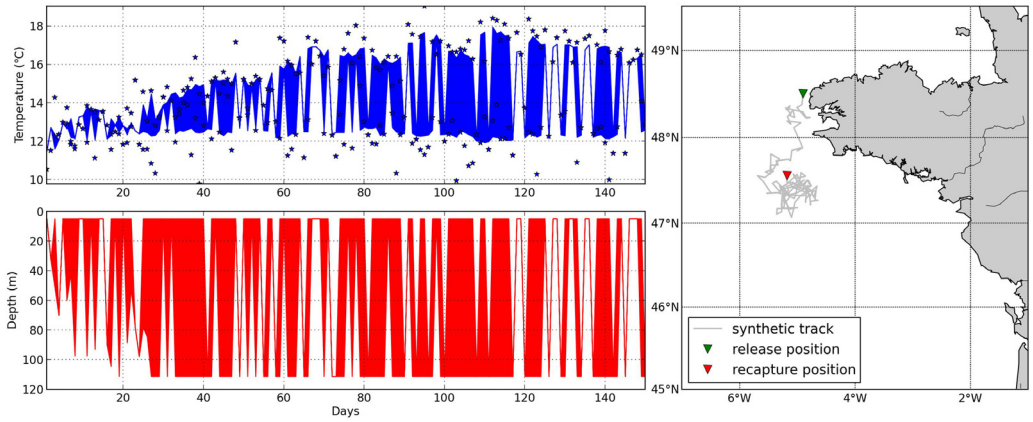

Fig. R1. (Top left) Simulated temperature history depicted by a blue polygon. Blue stars represent surface and bottom temperatures with observation errors. (Bottom left) Simulated depth history depicted by a red polygon. (Right) Simulated track in gray with release position (green triangle) and recapture position (red triangle). Simulated true values of the parameters were: $D = 30.0$, $\sigma_{surface} = 0.673$, and $\sigma_{bottom} = 1.050$. (For interpretation of the references to color in this figure legend, the reader is referred to the web version of this article).

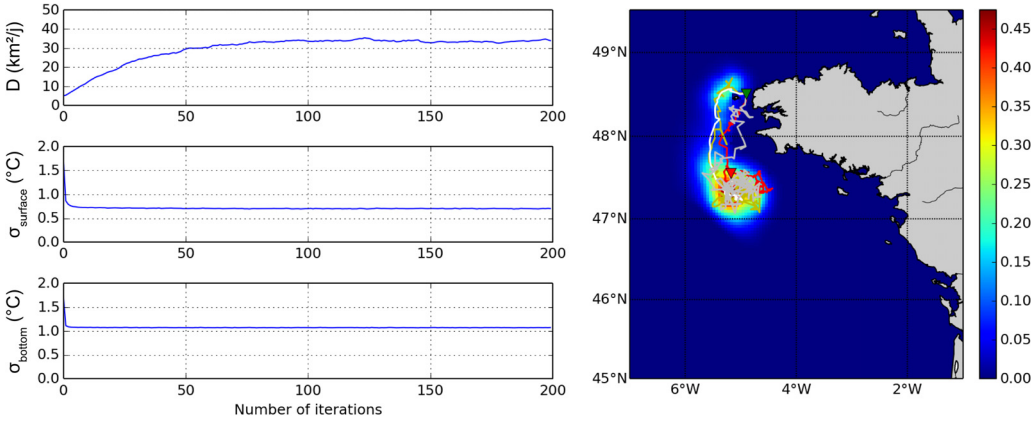

Fig. R2. (Left) Convergence of the SEM-based estimation of model parameters on synthetic data. (Right) Reconstruction of the simulated trajectory (gray line) illustrated with the posterior distribution summed over time (color image scale), the mean track (white line), the modal track (yellow line) and the most probable track (red line). (For interpretation of the references to color in this figure legend, the reader is referred to the web version of this article.)

Table R1
Simulated parameter values and estimated parameters for the synthetic data using the two different inference techniques. The gradient-based approach estimates only D with observation errors fixed either to the true values or that of the SEM estimates.

	D (km²/day)	$\sigma_{surface}$ (°C)	σ_{bottom} (°C)
Simulated true values	30.0	0.673	1.050
SEM-based ML estimates	33.8	0.697	1.070
Gradient-based ML estimate with observation errors set to the true values	32.4	0.673	1.050
Gradient-based ML estimate with observation errors set to the SEM estimates	31.2	0.697	1.070

inference capacity of the SEM procedure as well as the coherence between both approaches was checked for the remaining synthetic data. The performance of the SEM estimator was quantified over 100 simulations. Two metrics were considered: the coefficient of variation (CV) and the 95% credible interval (CI) of the parameter estimates (Table R2). In Bayesian statistics, a credible interval is an interval in the domain of a posterior probability distribution of the parameter, which differs from the frequentist confidence interval. The CV was higher for the coefficient of diffusion than for the observation errors (42% vs 7%). Then, all parameters estimates were within the 95% CI meaning that they were unbiased.

3.2. Model calibration and inference for real data

Daily DST temperature and depth series from a representative fish (tag A05392) was used as a real case study. The model parameters were estimated using the SEM procedure. The algorithm converged after about 50 iterations (Fig. R3). The estimated model parameters were $D = 27.3$, $\sigma_{surface} = 0.367$, and $\sigma_{bottom} = 1.859$. The reconstructed tracks according to the different criterion (MAP, MPM and mean tracks) looked consistent to one another, i.e., close to each other over the time series (Fig. R3). In addition, the reconstructed tracks seemed plausible relative to the sea bass ecology. Thus, over a year of data (383 days), the tagged fish spent some time in the Iroise Sea, then undertook a migration toward the south-east in the Bay of Biscay, stayed there for a while, and moved back to the Iroise Sea, thus completing a annual migration cycle. With observation errors set to the typical uncertainty levels, the gradient-based ML estimate of D is 30.1 km²/day. The two techniques of calibration and inference result in some small discrepancies in the estimated parameters, however, the reconstructed trajectory patterns were coherent (not shown). To ascertain that the trajectory reconstructed by our geolocation model is robust, one must assess

Table R2
Average of true parameter values and metrics of estimation performance (i.e., mean, standard deviation, coefficient of variation (CV) and credible interval (CI)) computed over 100 simulations.

Parameters	Average of true values	Mean	Std.	CV (%)	Lower 95% CI	Upper 95% CI
D	29.69	26.74	11.40	43	8.57	48.68
σ_{surface}	0.643	0.668	0.047	7	0.589	0.766
σ_{bottom}	0.994	1.045	0.083	8	0.906	1.201

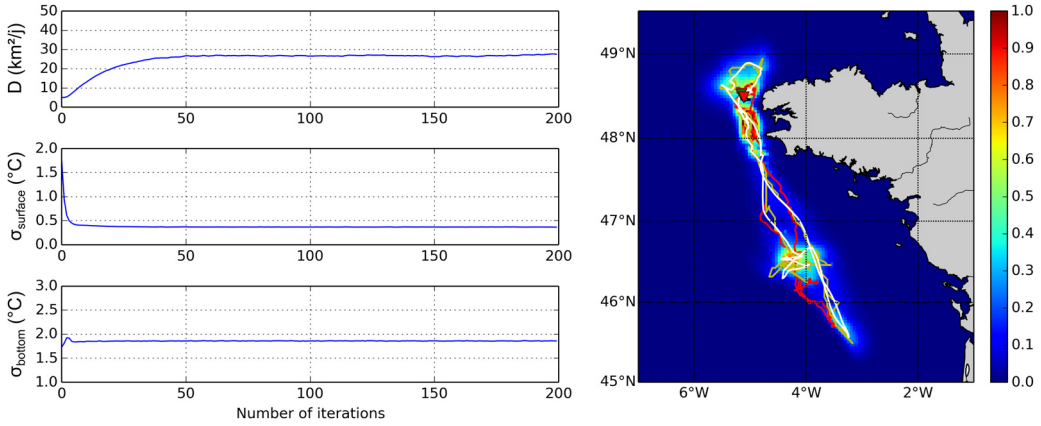

Fig. R3. (Left) Convergence of the SEM-based estimation of model parameters on the real data (tag A05392). (Right) Reconstruction of the trajectory illustrated with the posterior distribution summed over time (color image scale), the mean track (white line), the modal track (yellow line) and the most probable track (red line). (For interpretation of the references to color in this figure legend, the reader is referred to the web version of this article).

its sensitivity to the various model parameters, the geophysical reference fields and the recapture location.

3.3. Sensitivity analysis

First, the sensitivity to model parameters was evaluated by inferring trajectories for different sets of model parameters. Practically, 3 nominal values of D, σ_{surface} and σ_{bottom} were chosen in a range encompassing gradient-based ML estimates of D and typical uncertainty levels for the observation errors. The trajectories were reconstructed using these 9 possible sets of model parameters (Fig. R4). Posterior distributions summed over time were compared to the one reconstructed with the reference nominal parameter values (i.e., $D = 30$, $\sigma_{\text{surface}} = 0.55$ and $\sigma_{\text{bottom}} = 1.73$). To compare pairwise maps, the difference in log scale between cumulated probabilities was computed for each grid cell. Basic statistics as mean, variance and coefficient of variation (CV) were derived (Table R3). We observed that the posterior distribution summed over time spread in space with the increase of the observation errors and the diffusion coefficient. The trajectory patterns were modified locally but not globally. Given the nominal parameter values, the shrinking of the posterior distribution summed over time were larger in average (negative mean values) and more variant with the decrease of the coefficient of diffusion, then the observation error at the surface, finally the observation error at the bottom. The spreading of the posterior distribution summed over time was larger in average (positive mean values) and more variant with the increase of the coefficient of diffusion, then with the observation error at the surface, and the observation error at the bottom.

Second, the sensitivity to geophysical reference fields was evaluated. We inferred trajectories using either satellite-derived SST or MARS SST. The use of different geophysical fields for the SST makes a noticeable difference in the inferred trajectories (Fig. R5). When using satellite based SST, inferred trajectory pattern showed an entire migration cycle going toward the south and then back to the North. One can note two zones where the fish staid longer (one in the Iroise Sea and one in the South). In between these zones, the fish moved rapidly and in an oriented manner. By comparison, when using MARS SST, the inferred trajectory did not show such pattern. The trajectory was still cyclic, but this time the fish movement was more regular along the trajectory except at the end. In addition, the fish went less South and more toward the West. The use of observations (satellite-based SST) over model outputs (MARS-based SST) were eventually favored as the satellite data are more precise, and the reconstructed tracks with satellite-based SST were more coherent (MAP, MPM and mean track close to each other) than with models outputs. Given this analysis, the two zones where the fish stayed longer were interpreted as feeding and spawning grounds, whereas the rapid move between zones were interpreted as fish migration.

Last, the sensitivity to the presence/absence of recapture location was evaluated. For two representative tags, the trajectories were reconstructed with and without the recapture location (Fig. R6). We observed that the inferred trajectories did not show important differences in both cases. The general trajectory patterns were conserved. Only the last days of the trajectories showed some differences, demonstrating that the geolocation model was robust.

4. Discussion

4.1. Inference method

A HMM-based model allowing the undersea geolocation from Temperature-Depth DSTs has been successfully implemented for the first time. It can be regarded as an extension of the model developed by Pedersen et al. (2008). In comparison, it has the advantage of jointly estimating all model parameters, i.e., the coefficient of diffusion of the dynamical model, as well as the errors of the observation model. To achieve the joint estimation of movement and observation parameters, we consider a stochastic version of the EM algorithm for three main reasons. First, it might be stressed that EM procedures can be regarded as gradient-based optimizers. Different studies have compared convergence properties of EM and classical gradient-based optimizers. For instance, Minami (2004) reports the good global convergence properties of the EM

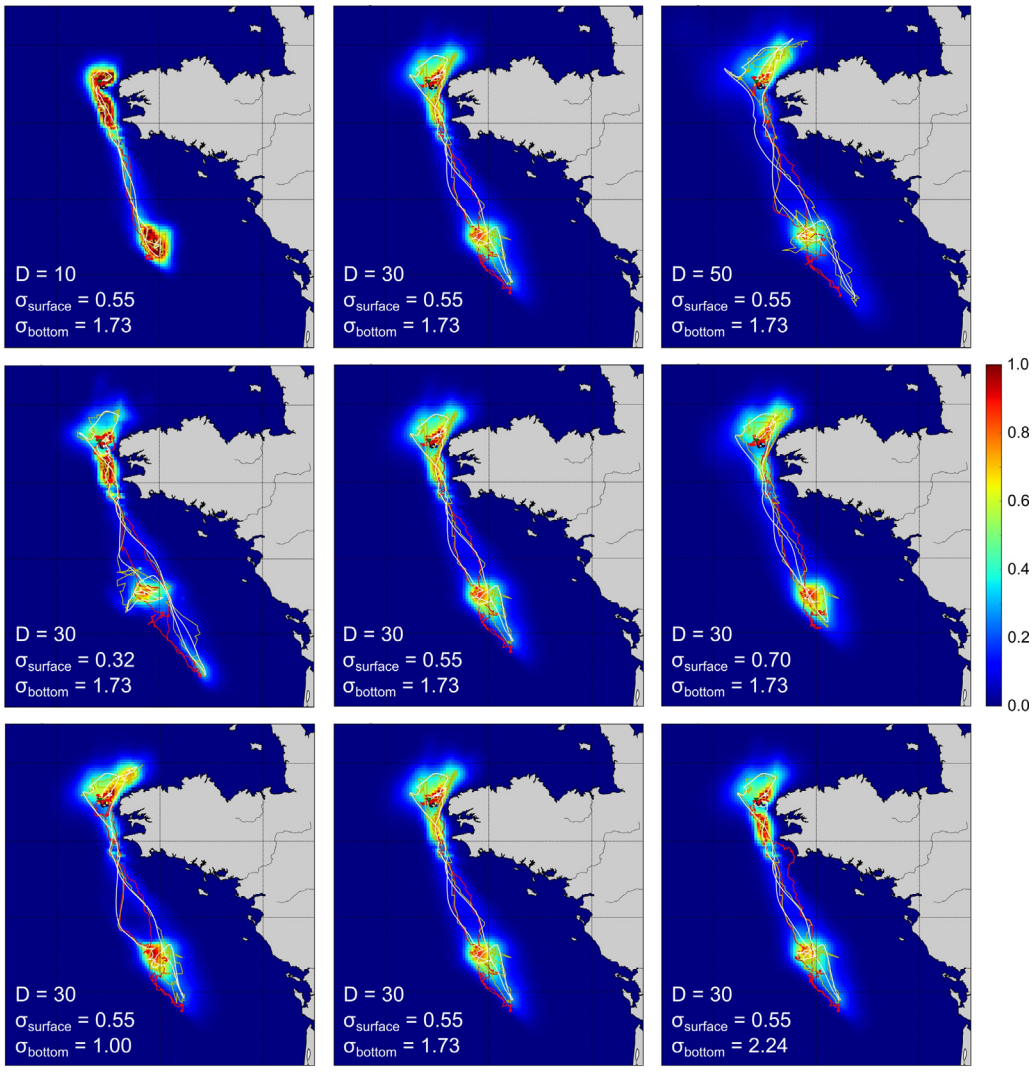

Fig. R4. Maps of posterior distributions summed over time with trajectories (mean, MPM and MAP) reconstructed based on different sets of parameters (3 values for D, 3 values for $\sigma_{surface}$ and 3 values for σ_{bottom}). (For interpretation of the references to color in this figure legend, the reader is referred to the web version of this article).

Table R3
Basic statistics (mean, variance, and coefficient of variation) computed from the difference between map of the posterior distributions summed over time of the reference nominal trajectory and that of the nominal trajectories. Note that cumulated probabilities of the posterior distributions were considered in log scale.

Nominal trajectories			Reference nominal trajectory			Mean	Variance	Coefficient of variation (%)
D	$\sigma_{surface}$	σ_{bottom}	D	$\sigma_{surface}$	σ_{bottom}			
10	0.55	1.73	30	0.55	1.73	−53.16	5445.10	−139
50	0.55	1.73	30	0.55	1.73	15.51	552.16	151
30	0.32	1.73	30	0.55	1.73	−10.02	421.56	−205
30	0.70	1.73	30	0.55	1.73	3.84	69.71	217
30	0.55	1.00	30	0.55	1.73	−2.94	33.06	−196
30	0.55	2.24	30	0.55	1.73	1.53	11.21	219

algorithm but greater convergence speed of quasi-Newton optimizer. Second, an interesting feature of the stochastic EM algorithm for the considered geolocation model is that it relies on previously developed model components namely the sampling of the posterior distribution of the state-sequence using a forward–backward procedure (Pedersen, 2007; Pedersen et al., 2008), and the ML estimation of observation and movement model parameter. As such, it does not require additional derivations of the first- and second-order as required by classical gradient-based techniques. Third, all deterministic gradient-based techniques are strongly dependent on the initialization of model parameters. The stochastic EM procedure ensures a greater robustness to these initial parameter values. This improves the convergence to the global solution, and avoids the reconstruction to be caught in a local solution.

Then, the joint estimation allowed having no *a priori* assumptions on model parameter values. This was in agreement with the lack of knowledge available in the natural environment for the most sensitive model parameter, the coefficient of diffusion (Fig. R4 and Table R3). Only maximum swimming speed of juvenile sea bass from a controlled environment were accessible (Killen et al., 2014),

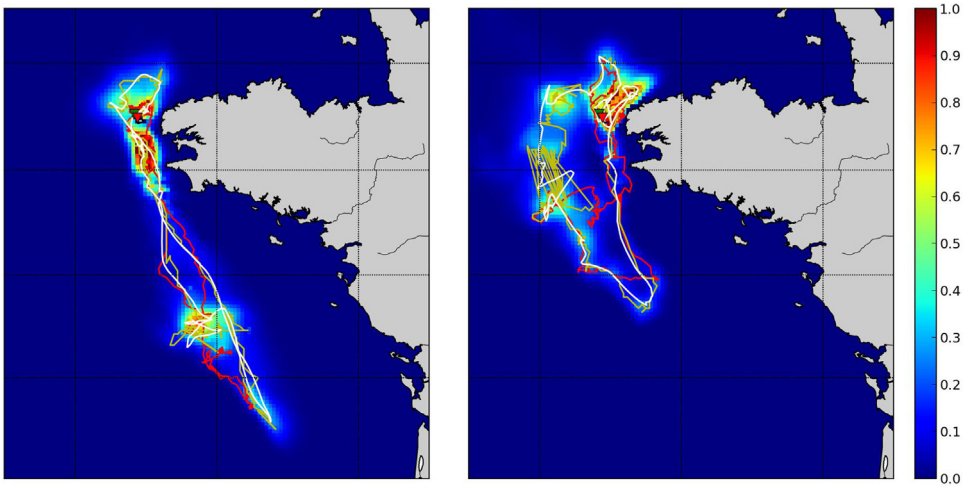

Fig. R5. (Left) Reconstructed trajectory using satellite data for the sea surface temperature. (Right) Reconstructed trajectory using MARS 3D model data for the sea surface temperature. (For interpretation of the references to color in this figure legend, the reader is referred to the web version of this article).

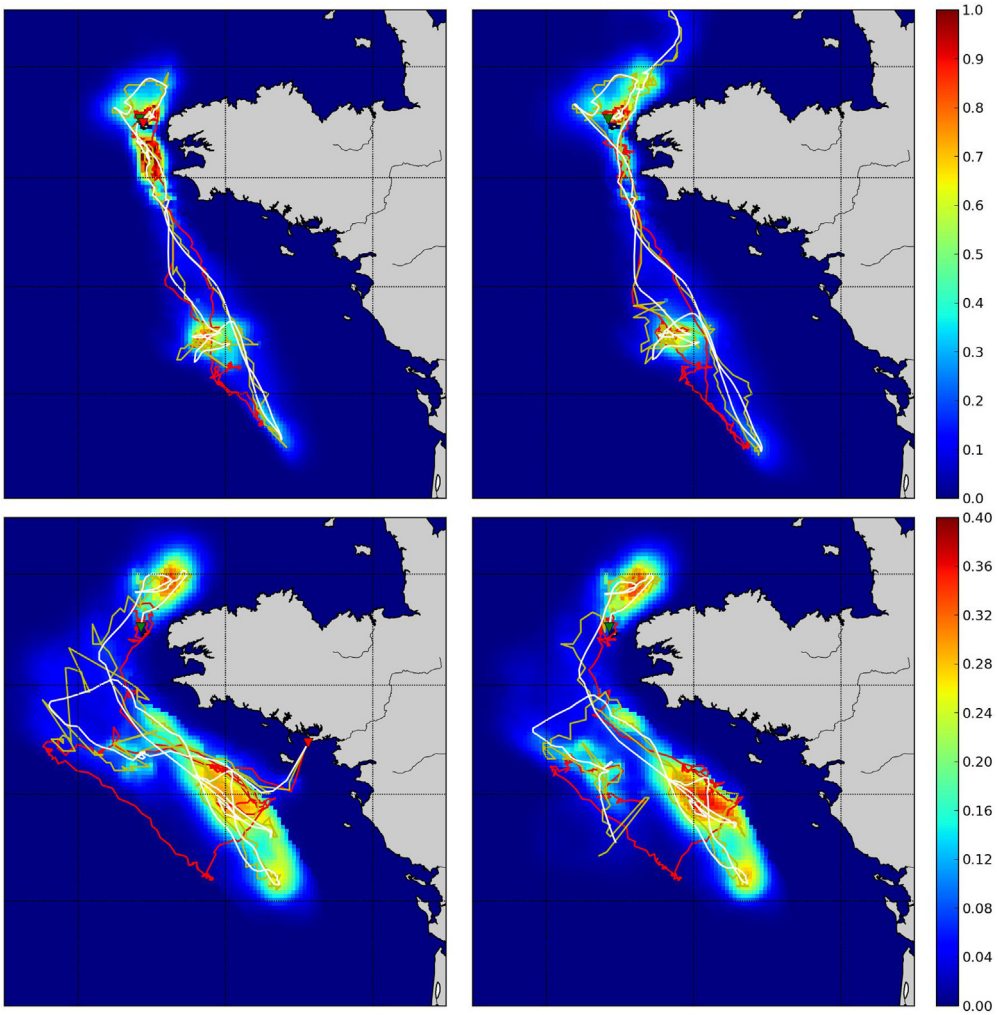

Fig. R6. Sensitivity to the recapture location for 2 real trajectories (tag A05392 on the top line, and tag A06226 on the bottom line): Map of posterior distributions summed over time with recapture positions (red triangle) on the left column and without on the right column. (For interpretation of the references to color in this figure legend, the reader is referred to the web version of this article).

which was not satisfactory. For the observation errors, the typical levels of uncertainty were provided with the satellite and model output data, however, these values were averages in space and time over a large domain, which might not be relevant locally when reconstructing trajectories (e.g., impact of clouds on the local error). Otherwise, the undersea geolocation is achieved using sea temperature and depth rather than tide signals as in Pedersen et al. (2008). Tide signals were not appropriate in our case first because

the sea bass seldom shows demersal behavior (with clear tidal signal on depth time series), and second because the Bay of Biscay does not have contrasted phase and amplitude tidal signals as observed in the North Sea. For these reasons, the sea temperature was considered as it revealed contrasted geophysical conditions allowing the reconstruction of the trajectory of an active swimmer fish. However, no behavioral switches were included in our geolocation model in order to develop our inference method in a simpler framework. The model is robust to model parameters as demonstrated by the sensitivity analysis with the convergence of the by-product trajectories (mean, MPM and MAP tracks).

4.2. Observation model

In the hidden Markov model framework, the observation model relates at every time step the extent to which the observation and the state (here the position) are coherent. Here, sea temperature and depth series were used as observation variables. However various other variables were used for more general trajectory reconstruction problems with or without irregularly recorded error-prone positions. As detailed hereafter, each observation variable and associated geophysical field has its pros and cons. Light-based geolocation is mostly adapted for transoceanic migrations (Musyl et al., 2001; Royer et al., 2005). Tide-based geolocation required environments where the phase and amplitude of the tidal signals are contrasted within the study area such as the North Sea for instance (Pedersen et al., 2008). In addition, fish need to exhibit resting periods where tide signals can be recorded with the pressure sensors. Regarding temperature-based geolocation, its success may depend on the contrast exhibited by the water masses explored by the fish. In other words, it required fish moving in water masses showing significant temperature gradients. That is the reason why our observation model is based on daily minimum and maximum temperature per depth layer. Alternative statistics could have been considered to summarize the daily temperature explored by the fish, but they would not maximize temperature contrast as much as the extreme values. Among the geophysical parameters of interest, salinity also appears as a relevant variable to infer fish movement in coastal or estuarine areas, especially when addressing diadromous species movement ecology. To our knowledge, only one application reported the use of salinity observations to geolocate fish (Pedersen et al., 2011b). The combination of several observation variables (temperature, tide signals and salinity) is also an appealing future direction to increase the precision of the reconstruction in areas where it is relevant (e.g., in the English channel and in the North Sea).

The reconstruction from synthetic data showed that the geolocation model performed well. For real data, the model appeared robust to the absence of recapture position. This is quite important, as tags are not always recovered where the fish dies (e.g., captured by professional or recreational fishermen). Thanks to a lightly buoyant flotation “jackets”, tags can be found stranded on the beach by hikers or within the seafood industry without the possibility to trace the fish back to the fisherman. In both cases, fish death can be inferred retrospectively, and the reconstruction is still doable increasing significantly the number of reconstructed tracks.

The model was also robust to model parameters, however, the reconstruction may be affected through several other aspects. Contrary to synthetic data, real data present some days where the fish is only in one of the layers (surface or bottom layer), or worse in none of them (i.e., between the surface and the bottom for an entire day). For the former, the observation likelihood is resolved only with one temperature field instead of two, unlike the latter, for which no observation are available, and the likelihood is equally probable all over the domain. These aspects have a negative impact on the reconstruction. Specifically, the more the proportion of days with no layers visited by the fish relative to the total days at liberty is high, the more uncertain the reconstruction will be. The proportion of days spent in 0, 1 and 2 layers can be used as an index to specify the quality of the reconstruction. For the representative tags considered for this study, these proportions were respectively 0.8%, 61.3% and 37.9% for the tag A05392, and 2.8%, 30.0% and 67.2% for the tag A06226. Although there were some undetermined days, the number of days with 1 or 2 layers visited was high enough to achieve a coherent reconstruction, as stressed by the sensitivity analysis.

Furthermore, we pointed out that the type of reference geophysical fields (satellite-based SST vs MARS-based SST) has an impact on the reconstruction. As stated earlier, observation data should be favored over model outputs. In the proposed implementation, we considered a simple Gaussian observation model. More advanced statistical models may be investigated to better account for the different types of noise and uncertainties (e.g., potential low-consistency patterns between the satellite-derived and MARS SST fields, differences between the very superficial temperature conditions measured by the satellite and the temperature conditions in the upper sea layer (0–10 m), diurnal sea surface temperature cycles,. . ..). The calibration of these models could combine both prior calibration from in situ datasets (for instance, for possible temperature offsets between the surface and the subsurface) as well as model parameter inference from the processed DST data.

Regarding the depth observation model, our approach disregards the uncertainty inherent in comparing the depth observation with the bathymetry. The depth observation from the tag has a minor uncertainty, but the main uncertainty comes from the potential variability of the bathymetry within a grid cell. The bathymetry is a 4 km $\times$ 4 km grid. Because of this size it is very unlikely that the seabed is flat within each grid cell. It is more likely that the value in a grid cell of the 4 km $\times$ 4 km bathymetry map represents some mean depth contained within the grid cell. Using the current depth model a problem arises if the fish visited a deep part of the grid cell. In the comparison with the bathymetry the grid cell would be excluded because the observed depth was deeper than the mean of the cell (or whatever the cell value represents) thus imposing a small bias in the geolocation. A more continuous approach (as in Pedersen, 2007; Pedersen et al., 2008) for the depth data likelihood could resolve this, either through the estimation of this uncertainty prior to running the model, or by including the uncertainty within the current estimation framework. Here, a parameter-free binary likelihood with a threshold set to the local bathymetry was considered to keep the model as simple as possible. This binary model could also account for some depth uncertainty by setting the threshold to a percentage greater than the local bathymetry (e.g., 110%, 120% depending on priors on the uncertainty level. . .). Numerical experiments have shown no significant changes with such parameterization. A continuous depth model (as in Pedersen, 2007; Pedersen et al., 2008), including some margin parameter, could also be considered and calibrated using the SEM algorithm. It will involve the same E-step and will complement the M-step with the update of depth parameters according to a weighted ML criterion. Future work could address this issue. However, as stated above, for the considered case-studies, we do not expect significant added-value from such a model as the depth information is rather a secondary cue compare to the temperature information.

Given the uncertainty on the recapture information, the SEM also delivers as a by-product the posterior variance of the recapture position. Contrary to movement and temperature model parameters, we did not update the variance of the recapture position from the posterior variance within each EM iteration. Additional experiments with this update could be undertaken in a future work; however, we are not expecting any significant global change in

the reconstructed trajectories, as demonstrated in the sensitivity analysis to the recapture location.

4.3. Dynamical model

The dynamical model described the time dynamics of the positions of the fish. In our case, such dynamics were ruled by one parameter, the coefficient of diffusion. As such, we considered a simple constant (constant mean velocity) and isotropic (no preferred movement orientation) prior model. This is a rather simple dynamics when modeling a migratory species such as the European sea bass (Pawson et al., 1987). Indeed, movement characteristics are expected to vary depending on the activities of the fish. For instance, the movement steps during foraging activity are more likely to be short and omnidirectional (Barraquand and Benhamou, 2008), whereas they might be large and oriented during migration behavior (Bowler and Benton, 2005). An alternative model could thus include some behavioral switches like in Pedersen et al. (2008). In this study, they estimated an activity level as a time-continuous indicator function to rule cod behavioral switches. The estimation was done before the geolocation step, because the distinction between different behaviors was obvious and it allowed preserving the tractability of the problem. For the sea bass, the behavioral switches could be derived from a joint analysis of horizontal and vertical data. Because in this case the distinction may not be obvious, the HMM setting should involve an additional latent variable referring to some hidden behavioral state (Pedersen et al., 2011a). Such an approach would significantly increase the computational complexity but appears tractable. The behavioral inference based on Hidden Markov models is quite common and recommended in other domains, for instance in marine ecology (Patterson et al., 2009; Pedersen et al., 2011a) or in fisheries (Vermard et al., 2010; Walker and Bez, 2010; Joo et al., 2013; Gloaguen et al., 2015). Alternative implementations based for instance on an augmented particle filter (Breed et al., 2012) also exist, but they may be less appropriate than the discrete HMM setting as detailed herein. Overall, the development of different geolocation models (with and without behavioral switches) will naturally raise the question of the respective performance of these models. Within a classical approach based on the Bayes theorem, which geolocation model provides the best reconstruction result may be answered by inspecting the likelihood of the residuals and keeping the model which depicts some optimal trade-off between the maximization of this likelihood and model complexity. Classically, this can be done computing the commonly used information criteria such as the Bayesian or the Aikaike's Information Criterion (BIC, AIC).

5. Conclusions

A HMM-based model allowing the undersea geolocation from Temperature-Depth DSTs has been successfully implemented for the first time. The implemented SEM algorithm provides an efficient and robust solution to infer all geolocation model parameters (i.e., both the observation errors and the coefficient of diffusion). The reconstructions for both synthetic and real data were robust. Geolocation results stressed the relevance of satellite-derived SST, compared to numerical hydrodynamic model outputs and we reported, for the first time, consistent reconstructions of sea bass migratory patterns within the Bay of Biscay. This method is generic and could be applied to the geolocation and tracking of many other pelagic fish such as tuna, salmon, shark or ray. Such geolocation models are particularly relevant to better understand the spatial dynamics and structuring of fish populations, which may improve fish stock delineations often poorly addressed in current management framework.

Acknowledgements

This study was partly funded by the Parc Naturel Marin d'Iroise (Agence des Aires Marines Protégées, convention Ifremer/PNMI, no. 10/2 211 451). The authors thank Ifremer staff (especially F. Garren and S. Martin) as well as PNMI staff (especially C. Laspougeas), fishers and stake holders for assistance in fish tagging and recapture. The authors also thank the 2 anonymous reviewers for their constructive comments that helped improve the manuscript. Satellite data were obtained from the Centre de Recherche et d'Exploitation Satellitaire (CERSAT), at IFREMER, Plouzané (France) on behalf of ESA/Medspiration project. MARS3D hydrodynamic model outputs were provided by the project PREVIMER.

Appendix A. Derivation of the updating equations (M-step) of the SEM algorithm.

This appendix shows that the M-step of the SEM algorithm comes to compute ML (Maximum Likelihood) estimates of model parameters from the trajectories sampled during the E-step (cf. Section 2.4). The SEM algorithm comes to iteratively maximize the expectation of the joint log-likelihood of the observations and the states conditionally to the posterior distribution for the current parameter estimates (Eq. (9) in the manuscript):

$$\hat{\Theta} = \underset{\Theta}{\operatorname{argmax}} \; E_{X|Y,\Theta^{(\nu)}} \left[\log p \left((Y_t)_{t=0:N-1}, (X_t)_{t=0:N-1} | \Theta \right) \right]$$

It resorts to solve:

$$\theta^{(\nu+1)} = \underset{\Theta}{\operatorname{argmax}} \int \log \left[p \left((Y_t)_{t=0:N-1}, (X_t)_{t=0:N-1} | \Theta \right) \right] \times p \left((X_t)_{t=0:N-1} | (Y_t)_{t=0:N-1}, \Theta^{(\nu)} \right) \mathrm{d}X$$

Considering an approximation of this integral from a sum over samples from posterior distribution $p\left((X_t)_{t=0:N-1}|(Y_t)_{t=0:N-1}, \Theta^{(\nu)}\right)$, the SEM algorithm amounts to:

$$\theta^{(\nu+1)} = \underset{\Theta}{\operatorname{argmax}} \sum_i \log \left[p \left((Y_t)_{t=0:N-1}, \left(X_t^{(i)}\right)_{t=0:N-1} | \Theta \right) \right]$$

where, $\left(X_t^{(i)}\right)_{t=0:N-1}$ are trajectories sampled from $p\left((X_t)_{t=0:N-1}|(Y_t)_{t=0:N-1}, \Theta^{(\nu)}\right)$ during the E-step of the SEM algorithm. Using the factorization of the joint log-likelihood $p\left((Y_t)_{t=0:N-1}, (X_t)_{t=0:N-1}|\Theta\right)$, we can decompose the above expression as:

$$\theta^{(\nu+1)} = \underset{\Theta}{\operatorname{argmax}} \sum_i \log \left[p \left((Y_t)_{t=0:N-1} | \left(X_t^{(i)}\right)_{t=0:N-1}, \Theta \right) \times p \left(\left(X_t^{(i)}\right)_{t=0:N-1} | \Theta \right) \right]$$

$$\theta^{(\nu+1)} = \underset{\Theta}{\operatorname{argmax}} \left[\sum_i \sum_t \log \left[p \left((Y_t)_{t=0:N-1} \middle| \left(X_t^{(i)}\right)_{t=0:N-1}, \sigma_{surface} \right) \right] + \sum_i \sum_t \log \left[p \left((Y_t)_{t=0:N-1} \middle| \left(X_t^{(i)}\right)_{t=0:N-1}, \sigma_{bottom} \right) \right] + \sum_i \sum_t \log \left[p \left(\left(X_t^{(i)}\right)_{t=0:N-1} \middle| \left(X_{t-1}^{(i)}\right)_{t=0:N-1}, D \right) \right] \right]$$

with $\Theta = (\sigma_{\text{surface}}, \sigma_{\text{bottom}}, D)$

Under modeling assumptions that surface and bottom temperature residuals follow a normal distribution and daily distance

increments follow a Rayleigh distribution with its variance equal to $2D$, we resort to three independent terms in the maximization:

$$\theta^{(\nu+1)} = \underset{\Theta}{\operatorname{argmax}} \left[\sum_i \sum_t \left[-\frac{1}{2}\log(2\pi) - \frac{1}{2}\log\left(\sigma^2_{\text{surface}}\right) \right] + \frac{1}{2\sigma^2_{\text{surface}}} \left(\text{SST}(X_t, T_t, D_t) - \text{SST}_{\text{SAT}}\left(X_t^{(i)}\right) \right)^2 \right] + \sum_i \sum_t \left[-\frac{1}{2}\log(2\pi) - \frac{1}{2}\log\left(\sigma^2_{\text{bottom}}\right) + \frac{1}{2\sigma^2_{\text{bottom}}} \left(\text{SBT}(X_t, T_t, D_t) - \text{SST}_{\text{MARS}}\left(X_t^{(i)}\right) \right)^2 \right] + \sum_i \sum_t \left[\log\left(X^{(i)}_{t+1} - X^{(i)}_t\right) - \log(2D) + \frac{\left(X^{(i)}_{t+1} - X^{(i)}_t\right)^2}{4D} \right] \right]$$

Setting the partial derivative with respect to each model parameters to 0, we derive the parameter updates:

$$\frac{\partial}{\partial \sigma_{\text{surface}}} : \sum_i \sum_t \left[-\frac{1}{2\sigma^{2(\nu+1)}_{\text{surface}}} + \frac{1}{2\sigma^{4(\nu+1)}_{\text{surface}}} \times \left(\text{SST}(X_t, T_t, D_t) - \text{SST}_{\text{SAT}}\left(X_t^{(i)}\right) \right)^2 \right] = 0$$

$$-\frac{N_{\text{SEM}} N}{2\sigma^{2(\nu+1)}_{\text{surface}}} + \frac{1}{2\sigma^{4(\nu+1)}_{\text{surface}}} \sum_{i=1}^{N_{\text{SEM}}} \sum_{t=0}^{N-1} \left(\text{SST}(X_t, T_t, D_t) - \text{SST}_{\text{SAT}}\left(X_t^{(i)}\right) \right)^2 = 0$$

$$\frac{1}{2\sigma^{4(\nu+1)}_{\text{surface}}} \sum_{i=1}^{N_{\text{SEM}}} \sum_{t=0}^{N-1} \left(\text{SST}(X_t, T_t, D_t) - \text{SST}_{\text{SAT}}\left(X_t^{(i)}\right) \right)^2 = \frac{N_{\text{SEM}} N}{2\sigma^{2(\nu+1)}_{\text{surface}}}$$

$$\sigma^{2(\nu+1)}_{\text{surface}} = \frac{1}{N_{\text{SEM}} N} \sum_{i=1}^{N_{\text{SEM}}} \sum_{t=0}^{N-1} \left(\text{SST}(X_t, T_t, D_t) - \text{SST}_{\text{SAT}}\left(X_t^{(i)}\right) \right)^2$$

The development is the same for $\sigma^{2(\nu+1)}_{\text{bottom}}$. Regarding parameter D, we obtain:

$$\frac{\partial}{\partial D} : \sum_i \sum_t \left[\log\left(X^{(i)}_{t+1} - X^{(i)}_t\right) - \log\left(2D^{(\nu+1)}\right) - \frac{\left(X^{(i)}_{t+1} - X^{(i)}_t\right)^2}{4D^{(\nu+1)}} \right] = 0$$

$$-\frac{N_{\text{SEM}} N}{2D^{(\nu+1)}} - \sum_{i=1}^{N_{\text{SEM}}} \sum_{t=0}^{N-1} \left(X^{(i)}_{t+1} - X^{(i)}_t\right)^2 \frac{-1}{D^{2(\nu+1)}} \frac{1}{4} = 0$$

$$D^{(\nu+1)} = \frac{1}{4 N_{\text{SEM}} N} \sum_{i=1}^{N_{\text{SEM}}} \sum_{t=0}^{N-1} \left(X^{(i)}_{t+1} - X^{(i)}_t\right)^2$$

Overall, the M-step of the SEM procedure comes to update model parameters as:

$$D^{(\nu+1)} = \frac{1}{4 N_{\text{SEM}} N} \sum_{i=1}^{N_{\text{SEM}}} \sum_{t=0}^{N-1} \left(X^{(i)}_{t+1} - X^{(i)}_t\right)^2$$

$$\sigma_s^{(\nu+1)} = \sqrt{\frac{1}{N_{\text{SEM}} N} \sum_{i=1}^{N_{\text{SEM}}} \sum_{t=0}^{N-1} \left(\text{SST}(X_t, T_t, D_t) - \text{SST}_{\text{SAT}}\left(X_t^{(i)}\right) \right)^2}$$

$$\sigma_b^{(\nu+1)} = \sqrt{\frac{1}{N_{\text{SEM}} N} \sum_{i=1}^{N_{\text{SEM}}} \sum_{t=0}^{N-1} \left(\text{SBT}(X_t, T_t, D_t) - \text{SST}_{\text{MARS}}\left(S_t^{(i)}\right) \right)^2}$$

It may be stressed that these updates may be regarded as the computation of the ML estimates from the trajectories sampled from the E-step. Hence, as mentioned in the main text, the SEM algorithm involves two procedures: the sampling of trajectories according to the posterior distribution $p\left((X_t)_{t=0:N-1} | (Y_t)_{t=0:N-1}, \Theta^{(\nu)}\right)$ (E-step) and the update of model parameters from ML estimates computed for the sampled trajectories (M-step). The later extend to any other observation and/or dynamical model. Hence, the SEM procedure provides an efficient and robust model calibration framework, while requiring no specific mathematical derivation.

References

Barraquand, F., Benhamou, S., 2008. Animal movements in heterogeneous landscapes: identifying profitable places and homogeneous movement bouts. Ecology 89, 3336–3348.

Baum, L.E., Petrie, T., Soules, G., Weiss, N., 1970. A maximization technique occurring in the statistical analysis of probabilistic functions of Markov chains. Ann. Math. Stat. 41, 164–171.

Bovet, P., Benhamou, S., 1988. Spatial analysis of animals' movements using a correlated random walk model. J. Theor. Biol. 131, 419–433.

Bowler, D.E., Benton, T.G., 2005. Causes and consequences of animal dispersal strategies: relating individual behaviour to spatial dynamics. Biol. Rev. Camb. Philos. Soc. 80, 205–225.

Breed, G.A., Costa, D.P., Jonsen, I.D., Robinson, P.W., Mills-Flemming, J., 2012. State-space methods for more completely capturing behavioral dynamics from animal tracks. Ecol. Model. 235–236, 49–58.

Dempster, A.P., Laird, N.M., Rubin, D.B., 1977. Maximum likelihood from incomplete data via the EM algorithm. J. R. Stat. Soc. Ser. B 39, 1–38.

Diebolt, J., Ip, E., Olkin, I., 1994. A Stochastic EM Algorithm for Approximating the Maximum Likelihood Estimate: Technical Report 301. Department of Statistics, Stanford University, California.

Do, C.B., Batzoglou, S., 2008. What is the expectation maximization algorithm? Nat. Biotechnol. 26, 897–899.

Doucet, A., Godsill, S., Andrieu, C., 2000. On sequential Monte Carlo sampling methods for Bayesian filtering. Stat. Comput. 10, 197–208.

Forney Jr., G.D., 1973. The viterbi algorithm. Proc. IEEE 61, 268–278.

Frimodt, C. (Ed.), 1995. Multilingual Illustrated Guide to the World's Commercial Coldwater Fish. , 1st edition. Wiley-Blackwell, Oxford, Cambridge, Mass., Cambridge, MA.

Gloaguen, P., Mahévas, S., Rivot, E., Woillez, M., Guitton, J., Vermard, Y., Etienne, M.P., 2015. An autoregressive model to describe fishing vessel movement and activity. Environmetrics 26, 17–28.

Holgate, P., 1971. Random walk models for animal behavior. Int. Symp. Stat. Ecol. N. Hav. 2, 1969.

ICES, 2015. Report of the ICES Advisory Committee. (No. ICES Advice, 2015. Book 5).

Johnson, D.S., London, J.M., Lea, M.-A., Durban, J.W., 2008. Continuous-time correlated random walk model for animal telemetry data. Ecology 89, 1208–1215.

Jonsen, I.D., Flemming, J.M., Myers, R.A., 2005. Robust state-space modeling of animal movement data. Ecology 86, 2874–2880.

Joo, R., Bertrand, S., Tam, J., Fablet, R., 2013. Hidden Markov models: the best models for forager movements? PLoS One 8, e71246.

Killen, S.S., Marras, S., McKenzie, D.J., 2014. Fast growers sprint slower: effects of food deprivation and re-feeding on sprint swimming performance in individual juvenile European sea bass. J. Exp. Biol. 217, 859–865.

Koutsikopoulos, C., Le Cann, B., 1996. Physical processes and hydrological structures related to the Bay of Biscay anchovy. Sci. Mar. 60, 9–19.

Lazure, P., Dumas, F., 2008. An external–internal mode coupling for a 3D hydrodynamical model for applications at regional scale (MARS). Adv. Water Resour. 31, 233–250.

Lazure, P., Garnier, V., Dumas, F., Herry, C., Chifflet, M., 2009. Development of a hydrodynamic model of the Bay of Biscay. Validation of hydrology. Cont. Shelf Res. 29, 985–997 (100 Years of Research within the Bay of Biscay XI International Symposium on Oceanography of the Bay of Biscay).

Minami, M., 2004. Convergence speed and acceleration of the EM algorithms, The EM Algorithm and Related Statistical Models, New York. In: Watanabe, M. and Yamaguchi, K. (Ed.), pp. 85–94.

Musyl, M.K., Brill, R.W., Curran, D.S., Gunn, J.S., Hartog, J.R., Hill, R.D., Welch, D.W., Eveson, J.P., Boggs, C.H., Brainard, R.E., 2001. Ability of archival tags to provide estimates of geographical position based on light intensity. In: Electronic Tagging and Tracking in Marine Fisheries. Kluwer, Dordrecht, pp. 343–367.

Nielsen, A., Bigelow, K.A., Musyl, M.K., Sibert, J.R., 2006. Improving light-based geolocation by including sea surface temperature. Fish. Oceanogr. 15, 314–325.

Patterson, T.A., Basson, M., Bravington, M.V., Gunn, J.S., 2009. Classifying movement behaviour in relation to environmental conditions using hidden Markov models. J. Anim. Ecol. 78, 1113–1123.

Pawson, M.G., Pickett, G.D., Kelley, D.F., 1987. The distribution and migrations of bass, *Dicentrarchus labrax* L., in waters around England and Wales as shown by tagging. J. Mar. Biol. Assoc. U.K. 67, 183–217.

Pedersen, M.W., 2007. Hidden Markov Models for Geolocation of Fish. Informatics and Mathematical Modelling, Technical University of Denmark (DTU), Richard Petersens Plads, Building 321, {DK-}2800 Kgs. Lyngby.

Pedersen, M.W., Righton, D., Thygesen, U.H., Andersen, K.H., Madsen, H., 2008. Geolocation of North Sea cod (*Gadus morhua*) using hidden Markov models and behavioural switching. Can. J. Fish. Aquat. Sci. 65, 2367–2377.

Pedersen, M.W., Patterson, T.A., Thygesen, U.H., Madsen, H., 2011a. Estimating animal behavior and residency from movement data. Oikos 120, 1281–1290.

Pedersen, M.W., Thygesen, U.H., Madsen, H., 2011b. Nonlinear tracking in a diffusion process with a Bayesian filter and the finite element method. Comput. Stat. Data Anal. 55, 280–290.

Piolle, J.-F., Autret, E., Arino, O., Robinson, I.S., Le Borgne, P., 2010. Medspiration: Toward the Sustained Delivery of Satellite SST Products and Services over Regional Seas. ESA Communications, Noordwijk.

Quayle, V.A., Righton, D., Hetherington, S., Pickett, G., 2009. Observations of the behaviour of European sea bass (*Dicentrarchus labrax*) in the North Sea. In: Nielsen, J., Arrizabalaga, H., Fragoso, N., Hobday, A., Lutcavage, M., Sibert, J. (Eds.), Tagging and Tracking of Marine Animals with Electronic Devices, Reviews: Methods and Technologies in Fish Biology and Fisheries. Springer, Netherlands, pp. 103–119.

Rabiner, L.R., 1989. A tutorial on hidden Markov models and selected applications in speech recognition. Proc. IEEE 77 (2), 257–286.

Risken, H., 1996. The Fokker-Planck Equation: (Methods of Solution and Applications). Springer Ser. Synerg.

Robert, C., 2007. The Bayesian Choice: From Decision Theoretic Foundations to Computational Implementation.

Royer, F., Fromentin, J.-M., Gaspar, P., 2005. A state–space model to derive bluefin tuna movement and habitat from archival tags. Oikos 109, 473–484.

Schurmann, H., Claireaux, G., Chartois, H., 1998. Change in vertical distribution of sea bass (*Dicentrarchus labrax* L.) during a hypoxic episode. Hydrobiologia 371–372, 207–213.

Sibert, J.R., Musyl, M.K., Brill, R.W., 2003. Horizontal movements of Bigeye tuna (*Thunnus obesus*) near Hawaii determined by Kalman filter analysis of archival tagging data. Fish. Oceanogr. 12, 141–151.

Vermard, Y., Rivot, E., Mahévas, S., Marchal, P., Gascuel, D., 2010. Identifying fishing trip behaviour and estimating fishing effort from VMS data using Bayesian hidden Markov models. Ecol. Model. 221, 1757–1769.

Viterbi, A.J., 1967. Error bounds for convolutional codes and an asymptotically optimum decoding algorithm. IEEE Trans. Inf. Theory 13, 260–269.

Walker, E., Bez, N., 2010. A pioneer validation of a state-space model of vessel trajectories (VMS) with observers' data. Ecol. Model. 221, 2008–2017.